Generalized Polarization Tensors for Shape Description*

Habib Ammari† Josselin Garnier‡ Hyeonbae Kang§
Mikyoung Lim¶ Sanghyeon Yu¶

November 10, 2011

Abstract

With each domain and material parameter, an infinite number of tensors, called the Generalized Polarization Tensors (GPTs), is associated. The GPTs contain significant information on the shape of the domain. In the recent paper [9], a recursive optimal control scheme to recover fine shape details of a given domain using GPTs is proposed. In this paper, we show that the GPTs can be used for shape description. We also show that high-frequency oscillations of the boundary of a domain are only contained in its high-order GPTs. Indeed, we provide a stability and resolution analysis for the reconstruction of small shape changes from the GPTs. By developing a level set version of the recursive optimization scheme, we make the change of topology possible and show that the GPTs can capture the topology of the domain. We provide numerical evidence that GPTs can capture topology and high-frequency shape oscillations. Both the analytical and numerical results of this paper clearly show that the concept of GPTs is a very promising new tool for shape description.

Mathematics Subject Classification (MSC2000): 35R30, 35B30

Keywords: generalized polarization tensors, shape description and representation, level-set, resolution and stability analysis

1 Introduction

The aim of this paper is to propose a new tool for shape description. Our tool is based on the concept of generalized polarization tensors (GPTs) introduced in [5]. The concept of GPTs occurs in several interesting contexts, in particular, in asymptotic models of dilute

*This work was supported by ERC Advanced Grant Project MULTIMOD–267184, National Research Foundation of Korea through grants No. 2009-0070442, 2010-0017532 and 2010-0004091, and Posco TJ Park foundation.

†Department of Mathematics and Applications, Ecole Normale Supérieure, 45 Rue d'Ulm, 75005 Paris, France (habib.ammari@ens.fr).

‡Laboratoire de Probabilités et Modèles Aléatoires & Laboratoire Jacques-Louis Lions, Université Paris VII, 75205 Paris Cedex 13, France (garnier@math.jussieu.fr)

§Department of Mathematics, Inha University, Incheon 402-751, Korea (hbkang@inha.ac.kr).

¶Department of Mathematical Sciences, Korean Advanced Institute of Science and Technology, Daejeon 305-701, Korea (mklim@kaist.ac.kr, shyu@kaist.ac.kr).

composites (see [21] and [12]), in invisibility cloaking in the quasi-static regime [8] and in potential theory related to certain questions arising in hydrodynamics [22].

Another important use of this concept is for imaging diametrically small inclusions from boundary measurements. In fact, the GPTs are the basic building blocks for the asymptotic expansions of the boundary voltage perturbations due to the presence of small conductivity inclusions inside a conductor [17, 2]. Based on this expansion, efficient algorithms to determine the location and some geometric features of the inclusions were proposed. We refer to [4, 5] and the references therein for recent developments of this theory.

There are many methods for shape description and representation [20]. Of particular interest are the global scalar transform techniques which compute a scalar result based on the global shape. Moment based methods are among the most popular and well-known global scalar transform methods, see, for instance, [24], [18], and [19].

In order to show the use of GPTs for shape description is an efficient global scalar transform technique, we first prove invariance properties of GPTs under translation, rotation, and scaling. Then we show that the GPTs capture high-frequency shape oscillations as well as topology. There is a (material) parameter in GPTs. It can be used as color so that GPTs can describe multiple connected domains with different colors. To handle topology changes, we implement a level set version of the recursive matching GPTs algorithm introduced in [9]. Moreover, we prove that high-frequency oscillations of the shape of a domain are only contained in its high-order GPTs and perform a stability and resolution analysis for the reconstruction of small shape changes from noisy GPTs. A generalization of the results of this paper to elastic GPTs [11, 5] (also called elastic moment tensors) would provide a new basis for shape description. This will be the subject of a forthcoming investigation.

2 Definition and basic properties of the GPTs

Throughout this paper we assume that the domains under consideration have $\mathcal{C}^2$-smooth boundaries and they are two dimensional. Let Γ be the fundamental solution to the Laplacian in two dimensions, *i.e.*,

$$\Gamma(x) = \frac{1}{2\pi} \ln |x|.$$

For a given bounded domain D in $\mathbb{R}^2$, the Neumann-Poincaré operator, $\mathcal{K}_D$, is defined for a density function $\phi \in L^2(\partial D)$ by

$$\mathcal{K}_D[\phi](x) = \frac{1}{2\pi} \int_{\partial D} \frac{\langle y - x, \nu(y) \rangle}{|x-y|^2} \phi(y) \, d\sigma(y),$$

where $\nu(y)$ is the outward unit normal to ∂D at $y \in \partial D$ and $\langle \, , \rangle$ denotes the scalar product in $\mathbb{R}^2$. Let $\mathcal{K}_D^*$ be the L^2-adjoint of $\mathcal{K}_D$, *i.e.*,

$$\mathcal{K}_D^*[\phi](x) = \frac{1}{2\pi} \int_{\partial D} \frac{\langle x - y, \nu(x) \rangle}{|x-y|^2} \phi(y) \, d\sigma(y).$$

It is well-known that for any real number λ with $|\lambda| > 1/2$ or $\lambda = -1/2$, $(\lambda I - \mathcal{K}_D^*)$ is invertible on $L^2(\partial D)$. Moreover, if $|\lambda| \geq 1/2$, then $(\lambda I - \mathcal{K}_D^*)$ is invertible on $L^2_0(\partial D) := \{f \in L^2(\partial D) : \int_{\partial D} f d\sigma = 0\}$. See, for instance, [16].

Let $|\lambda| > 1/2$. For a multi-index $\alpha = (\alpha_1, \alpha_2) \in \mathbb{N}^2$ where $\mathbb{N}$ is the set of all positive integers, define ϕ_α by

$$\phi_\alpha(y) := (\lambda I - \mathcal{K}_D^*)^{-1}\big[\nu(x)\cdot\nabla x^\alpha\big](y), \quad y \in \partial D. \tag{1}$$

Here and throughout this paper, we use the conventional notation: $x^\alpha = x_1^{\alpha_1}x_2^{\alpha_2}$, $|\alpha| = \alpha_1 + \alpha_2$.

The generalized polarization tensors (GPTs) $M_{\alpha\beta}$ for α, $\beta \in \mathbb{N}^2$ ($|\alpha|, |\beta| \geq 1$) associated with the parameter λ and the domain D are defined by

$$M_{\alpha\beta}(\lambda, D) := \int_{\partial D} y^\beta \phi_\alpha(y)\,d\sigma(y). \tag{2}$$

The GPTs are the building blocks in representing the perturbation of the electrical potential in the presence of an inclusion D of conductivity contrast k. The parameter λ is related to k via the formula

$$\lambda = \frac{k+1}{2(k-1)}. \tag{3}$$

Note that the GPTs are real valued tensors. Key properties of positivity and symmetry of the GPTs are proved in [5, Chapter 4]. We emphasize that what is important is not the individual terms $M_{\alpha\beta}$ but their harmonic combinations. A harmonic combination of GPTs is $\sum_{\alpha,\beta} a_\alpha b_\beta M_{\alpha\beta}$ where $\sum_\alpha a_\alpha x^\alpha$ and $\sum_\beta b_\beta x^\beta$ are (real) harmonic polynomials. We call such (a_α) and (b_β) (real) harmonic coefficients. Let us recall the following symmetry property:

$$\sum_{\alpha,\beta} a_\alpha b_\beta M_{\alpha\beta}(\lambda, D) = \sum_{\alpha,\beta} a_\alpha b_\beta M_{\beta\alpha}(\lambda, D) \tag{4}$$

for any pair (a_α), (b_β) of harmonic coefficients. Moreover, the following uniqueness result holds [3].

Proposition 2.1 *If all harmonic combinations of GPTs of two domains are the same, i.e.,*

$$\sum_{\alpha,\beta} a_\alpha b_\beta M_{\alpha\beta}(\lambda_1, D_1) = \sum_{\alpha,\beta} a_\alpha b_\beta M_{\alpha\beta}(\lambda_2, D_2)$$

for all pairs (a_α), (b_β) of harmonic coefficients, then $D_1 = D_2$ and $\lambda_1 = \lambda_2$.

Proposition 2.1 says that the full knowledge of (harmonic combinations of) GPTs determines the domain D and λ. It is known that the first order GPT, $M_{\alpha\beta}$ for $|\alpha| + |\beta| = 2$, yields the equivalent ellipse [13, 6, 5]. The equivalent ellipse of D is the ellipse with same first order GPTs as D. However, it is not known analytically what kind of information on D and λ the higher order GPTs carry. It is the purpose of this paper to exploit the possibility of using higher order GPTs for the shape description.

In relation to the widely used shape description from moments, we recall the following result from [5, Theorem 4.13] which says that the GPTs can be estimated from above and below in terms of the harmonic moments.

Proposition 2.2 *Let $f(y) = \sum_{\alpha \in I} a_\alpha y^\alpha$ be a harmonic polynomial. Then*

$$\frac{2}{2\lambda+1}\int_D |\nabla f|^2 \leq \sum_{\alpha,\beta\in I} a_\alpha a_\beta M_{\alpha\beta}(\lambda, D) \leq \frac{2}{2\lambda-1}\int_D |\nabla f|^2 \,. \tag{5}$$

We also recall the following monotonicity of $\sum_{\alpha,\beta} a_\alpha a_\beta M_{\alpha\beta}(\lambda, D)$ with respect to the domain [7].

Proposition 2.3 *Let $D \subsetneqq D'$. Then, for all (nonzero) harmonic coefficients $(a_\alpha)_{|\alpha|\geq 1}$,*

$$\sum_{\alpha,\beta} a_\alpha a_\beta M_{\alpha\beta}(\lambda, D) < \sum_{\alpha,\beta} a_\alpha a_\beta M_{\alpha\beta}(\lambda, D') \qquad \text{if } \lambda > \frac{1}{2},$$

and

$$\sum_{\alpha,\beta} a_\alpha a_\beta M_{\alpha\beta}(\lambda, D) > \sum_{\alpha,\beta} a_\alpha a_\beta M_{\alpha\beta}(\lambda, D') \qquad \text{if } \lambda < -\frac{1}{2}.$$

Particularly interesting choices of harmonic coefficients are those of homogeneous harmonic polynomials: for a positive integer n and a multi-index α with $|\alpha| = n$, define (a^n_α) by

$$\sum_{|\alpha|=n} a^n_\alpha x^\alpha = r^n e^{in\theta} = (x_1 + ix_2)^n, \tag{6}$$

where $x = (r, \theta)$ in polar coordinates. Using these (complex) harmonic coefficients, we introduce for positive integers m and n

$$M^c_{mn}(\lambda, D) = \sum_{|\alpha|=m} \sum_{|\beta|=n} a^m_\alpha a^n_\beta M_{\alpha\beta}(\lambda, D). \tag{7}$$

We call M^c_{mn} the contracted GPTs [8]. An efficient algorithm for computing the contracted GPTs is presented in [15].

3 Translation, rotation, and scaling properties of the GPTs

In this section we show new properties of the GPTs which are particularly useful for shape description. Let N be a postitive integer. We prove that the set of $(M_{\alpha\beta}(\lambda, D))$ for $|\alpha|+|\beta| \leq N$ is invariant under translation and rotation of D. We also provide a scaling formula for the GPTs.

3.1 Translation

For $T = (T_1, T_2)$, define $D^T := \{y + T : \; y \in D\}$ and $\partial D^T = (\partial D)^T$, and let $y^T = y + T$. For $\varphi \in L^2(\partial D)$, define $\varphi^T \in L^2(\partial D^T)$ as

$$\varphi^T(y^T) := \varphi(y), \quad \text{where } y \in \partial D.$$

Note that, for φ defined on ∂D, we have

$$\begin{aligned}
\mathcal{K}^*_{D^T}[\varphi^T](x^T) &= \frac{1}{2\pi} \int_{\partial D^T} \frac{\langle x^T - \tilde{y}, \nu(x^T)\rangle}{|x^T - \tilde{y}|^2} \phi^T(\tilde{y}) \; d\sigma(\tilde{y}) \\
&= \frac{1}{2\pi} \int_{\partial D} \frac{\langle x^T - y^T, \nu(x^T)\rangle}{|x^T - y^T|^2} \phi^T(y^T) \; d\sigma(y) \\
&= \mathcal{K}^*_D[\varphi](x).
\end{aligned}$$

For multi-index α and γ, let the coefficients $c^T_{\alpha\gamma}$ be such that

$$(x-T)^\alpha = \sum_\gamma c^T_{\alpha\gamma} x^\gamma, \quad \forall\, x \in \mathbb{R}^2. \tag{8}$$

It is worth mentioning that $c^T_{\alpha\gamma} = 0$ if $|\gamma| > |\alpha|$.

Let $\varphi_{D,\alpha}$ be the density function defined by (1) for a given domain D and multi-index α. Then we have for $x^T \in \partial D^T$

$$\begin{aligned}\Big(\lambda I - \mathcal{K}^*_{D^T}\Big)[\varphi^T_{D,\alpha}](x^T) &= \Big(\lambda I - \mathcal{K}^*_D\Big)[\varphi_{D,\alpha}](x)\\ &= \nu(x)\cdot\nabla x^\alpha\Big|_{\partial D}\\ &= \sum_\gamma c^T_{\alpha\gamma}\nu(x^T)\cdot\nabla(x^T)^\gamma.\end{aligned}$$

Hence,

$$\varphi^T_{D,\alpha} = \sum_\gamma c^T_{\alpha\gamma}\varphi_{D^T,\gamma} \quad \text{on } \partial D^T,$$

and the following proposition holds.

Proposition 3.1 *Let $D^T = \{y+T : y \in D\}$. Then,*

$$M_{\alpha\beta}(\lambda, D) = \sum_{\eta,\gamma} c^T_{\beta\eta} c^T_{\alpha\gamma} M_{\eta\gamma}(\lambda, D^T), \tag{9}$$

where the coefficients $c^T_{\beta\eta}$ and $c^T_{\alpha\gamma}$ are given by (8).

Proof. We compute

$$\begin{aligned}M_{\alpha\beta}(\lambda, D) &= \int_{\partial D} y^\beta \varphi_\alpha(y)\, d\sigma(y)\\ &= \int_{\partial D^T} (\tilde{y}-T)^\beta \varphi^T_{D,\alpha}(\tilde{y})\, d\sigma(\tilde{y})\\ &= \int_{\partial D^T} \sum_\eta c^T_{\beta\eta}\tilde{y}^\eta \sum_\gamma c^T_{\alpha\gamma}\varphi_{D^T,\gamma}\, d\sigma(\tilde{y}),\end{aligned}$$

to find

$$M_{\alpha\beta}(\lambda, D) = \sum_{\eta,\gamma} c^T_{\beta\eta} c^T_{\alpha\gamma} M_{\eta\gamma}(\lambda, D^T),$$

as desired. ■

For example, when $\alpha = (1,0)$ and $\beta = (2,0)$, we have $(x-T)^\alpha = x_1 - T_1$ and $(x-T)^\beta = (x_1-T_1)^2 = x_1^2 - 2T_1x_1 + T_1^2$, and readily get

$$M_{(1,0),(2,0)}(\lambda, D) = M_{(1,0),(2,0)}(\lambda, D^T) - 2T_1 M_{(1,0),(1,0)}(\lambda, D^T).$$

3.2 Rotation

For $y \in \mathbb{R}^2$, let $y_\theta = \begin{pmatrix} \cos\theta & -\sin\theta \\ \sin\theta & \cos\theta \end{pmatrix} \begin{pmatrix} y_1 \\ y_2 \end{pmatrix}$, *i.e.*, the rotation of y with angle θ with respect to the origin. Set $D_\theta = \{y_\theta : \ y \in D\}$ and

$$\varphi^\theta(y_\theta) := \varphi(y), \quad y \in \partial D.$$

Note that, for a density function φ defined on ∂D, we have

$$\begin{aligned} \mathcal{K}^*_{D_\theta}[\varphi^\theta](x_\theta) &= \frac{1}{2\pi} \int_{\partial D_\theta} \frac{\langle x_\theta - \tilde{y}, \nu(x_\theta)\rangle}{|x_\theta - \tilde{y}|^2} \phi^\theta(\tilde{y}) \ d\sigma(\tilde{y}) \\ &= \frac{1}{2\pi} \int_{\partial D} \frac{\langle x_\theta - y_\theta, \nu(x_\theta)\rangle}{|x_\theta - y_\theta|^2} \phi^\theta(y_\theta) \ d\sigma(y) \\ &= \mathcal{K}^*_D[\varphi](x). \end{aligned}$$

For multi-index α and γ, let the coefficients $r^\theta_{\alpha\gamma}$ be such that

$$(x_{-\theta})^\alpha = \sum_\gamma r^\theta_{\alpha\gamma} x^\gamma, \quad \forall\, x \in \mathbb{R}^2. \tag{10}$$

Again, it should be noted that $r^\theta_{\alpha\gamma} = 0$ if $|\gamma| > |\alpha|$. The following rotation formula for the GPTs can be proved in the same way as the translation formula (9).

Proposition 3.2 *Let $D_\theta = \{y_\theta : \ y \in D\}$. Then*

$$M_{\alpha\beta}(\lambda, D) = \sum_{\eta,\gamma} r^\theta_{\beta\eta} r^\theta_{\alpha\gamma} M_{\eta\gamma}(\lambda, D_\theta), \tag{11}$$

where the coefficients $r^\theta_{\beta\eta}$ and $r^\theta_{\alpha\gamma}$ are given by (10).

3.3 Scaling

Similarly, define for a positive real s, $D^s := \{sy : \ y \in D\}$ and set $\varphi^s(sy) = \varphi(y)$, $y \in \partial D$. Then, we have

$$\begin{aligned} \mathcal{K}^*_{D^s}[\varphi^s](x^s) &= \frac{1}{2\pi} \int_{\partial D^s} \frac{\langle x^s - \tilde{y}, \nu(x^s)\rangle}{|x^s - \tilde{y}|^2} \phi^s(\tilde{y}) \ d\sigma(\tilde{y}) \\ &= \frac{1}{2\pi} \int_{\partial D} \frac{\langle x^s - y^s, \nu(x^s)\rangle}{|x^s - y^s|^2} \phi^s(y^s) s \ d\sigma(y) \\ &= \mathcal{K}^*_D[\varphi](x). \end{aligned}$$

From

$$(s^{-1}x)^\alpha = \frac{1}{s^{|\alpha|}} x^\alpha, \quad \forall\, x \in \mathbb{R}^2,$$

the following holds.

Proposition 3.3 *Let $D^s := \{sy : \ y \in D\}$ for a positive real number s. Then*

$$M_{\alpha\beta}(\lambda, D) = \frac{1}{s^{|\alpha|+|\beta|}} M_{\alpha\beta}(\lambda, D^s). \tag{12}$$

4 Shape derivative of the GPTs

Let $D = \cup_{j=1}^J D_j$ where D_j is a bounded connected domain with $\mathcal{C}^2$-boundary. To each D_j, we associate $|\lambda_j| > 1/2$ and set $\lambda = (\lambda_1, \ldots, \lambda_J)$. The GPTs associated with the multiple inclusions $\cup_{j=1}^J D_j$ and λ can be defined similarly to the single inclusion case by using a system of integral equations. We do not give the definition here, instead we simply refer to [5, Section 4.10]. We emphasize that the translation, rotation, and scaling properties of the GPTs hold for multiple inclusions.

For ϵ small, let D_ϵ be an ϵ-deformation of D, *i.e.*, there are functions $h_j \in \mathcal{C}^1(\partial D_j)$, $1 \le j \le J$, such that

$$\partial D_\epsilon := \cup_{j=1}^J \{\tilde{x} = x + \epsilon h_j(x)\nu_j(x) \ : x \in \partial D_j\}, \tag{13}$$

where ν_j is the outward unit normal vector on ∂D_j. Suppose that a_α and b_β are constants such that $H(x) = \sum_\alpha a_\alpha x^\alpha$ and $F(x) = \sum_\beta b_\beta x^\beta$ are harmonic polynomials. Then, according to [9], the perturbation of a harmonic sum of GPTs due to the shape deformation is given as follows:

$$\begin{aligned}
&\sum_{\alpha,\beta} a_\alpha b_\beta M_{\alpha\beta}(\lambda, D_\epsilon) - \sum_{\alpha,\beta} a_\alpha b_\beta M_{\alpha\beta}(\lambda, D) \\
&= \sum_{j=1}^J \epsilon(k_j - 1) \int_{\partial D_j} h_j(x) \left[\frac{\partial u}{\partial \nu}\Big|_- \frac{\partial v}{\partial \nu}\Big|_- + \frac{1}{k_j} \frac{\partial u}{\partial T}\Big|_- \frac{\partial v}{\partial T}\Big|_- \right](x)\, d\sigma(x) + O(\epsilon^2),
\end{aligned} \tag{14}$$

where $k_j = (2\lambda_j + 1)/(2\lambda_j - 1)$ and u and v are respectively solutions to the (primal and dual) problems:

$$\begin{cases}
\Delta u = 0 & \text{in } D \cup (\mathbb{R}^2 \backslash \overline{D}), \\
u|_+ - u|_- = 0 & \text{on } \partial D_j,\ 1 \le j \le J, \\
\dfrac{\partial u}{\partial \nu}\Big|_+ - k_j \dfrac{\partial u}{\partial \nu}\Big|_- = 0 & \text{on } \partial D_j,\ 1 \le j \le J, \\
(u - H)(x) = O(|x|^{-1}) & \text{as } |x| \to \infty,
\end{cases} \tag{15}$$

and

$$\begin{cases}
\Delta v = 0 & \text{in } D \cup (\mathbb{R}^2 \backslash \overline{D}), \\
k_j v|_+ - v|_- = 0 & \text{on } \partial D_j,\ 1 \le j \le J, \\
\dfrac{\partial v}{\partial \nu}\Big|_+ - \dfrac{\partial v}{\partial \nu}\Big|_- = 0 & \text{on } \partial D_j,\ 1 \le j \le J, \\
(v - F)(x) = O(|x|^{-1}) & \text{as } |x| \to \infty.
\end{cases} \tag{16}$$

The shape derivative of GPTs can be easily derived using (14), see Section 6.

5 Stability and resolution analysis in the linearized case

Let D be the unit disk, $|\lambda| > 1/2$, and $k = (2\lambda + 1)/(2\lambda - 1)$. Let $F(x) = r^m e^{im\theta}$ and $H(x) = r^n e^{in\theta}$ for $m, n \in \mathbb{N}$. The solutions u_n and v_m of respectively (15) and (16) are given by

$$u_n(x) = \begin{cases} \dfrac{2}{1+k} r^n e^{in\theta}, & r < 1, \\ (\dfrac{1-k}{1+k}\dfrac{1}{r^n} + r^n) e^{in\theta}, & r > 1, \end{cases}$$

and

$$v_m(x) = \begin{cases} \dfrac{2k}{1+k} r^m e^{im\theta}, & r < 1, \\ (\dfrac{1-k}{1+k}\dfrac{1}{r^m} + r^m) e^{im\theta}. & r > 1. \end{cases}$$

Let D_ϵ be an ϵ-perturbation of D:

$$\partial D_\epsilon := \{\tilde{x} = x + \epsilon h(x)\nu(x) \ : x \in \partial D\},$$

where $h \in \mathcal{C}^1(\partial D)$. We use the Fourier convention

$$\hat{h}_p = \frac{1}{2\pi}\int_0^{2\pi} h(\theta) e^{-ip\theta}\, d\theta, \qquad h(\theta) = \sum_{p\in\mathbb{Z}} \hat{h}_p e^{ip\theta}.$$

Let $M^c_{mn}(\lambda, D_\epsilon)$ and $M^c_{mn}(\lambda, D)$ be the contracted GPTs associated with D_ϵ and D respectively. Since

$$\frac{\partial u_n}{\partial \nu}\Big|_- \frac{\partial v_m}{\partial \nu}\Big|_- + \frac{1}{k}\frac{\partial u_n}{\partial T}\Big|_- \frac{\partial v_m}{\partial T}\Big|_- = \frac{4(k-1)mn}{(k+1)^2} e^{i(m+n)\theta},$$

we obtain

$$M^c_{mn}(\lambda, D_\epsilon) - M^c_{mn}(\lambda, D) = 2\pi\epsilon \frac{mn}{\lambda^2}\hat{h}_{m+n} + O(\epsilon^2) \tag{17}$$

as $\epsilon \to 0$.

The asymptotic formula (17) shows that high-frequency oscillations of the boundary deformation of a disk-shaped inclusion are only contained in its high-order contracted GPTs. Moreover, only $\hat{h}_p$ for p up to $2N$ can be reconstructed from the set of contracted GPTs M^c_{mn} for $m, n \leq N$.

Now, let δ be a small parameter. Following [1], we perform from (17) a stability and resolution analysis for the reconstruction of h from noisy $M^c_{mn}(\lambda, \delta D_\epsilon)$ for $m, n \leq N$. For doing so, we introduce

$$a_{mn} = \frac{\lambda^2}{2\pi mn \delta^{m+n}}(M^c_{mn}(\lambda, \delta D_\epsilon) - M^c_{mn}(\lambda, \delta D)).$$

Assume that $M^c_{mn}(\lambda, \delta D_\epsilon)$ are corrupted with white noise. Thus,

$$a^{\text{meas}}_{m,n} = a_{mn} + \sigma W_{m,n},$$

with the noise terms $W_{m,n}$ modeled as independent standard complex circularly symmetric Gaussian random variables such that

$$\mathbb{E}[|W_{m,n}|^2] = \frac{e^{2\kappa(m+n)}}{m^2 n^2}, \tag{18}$$

σ thus modeling the noise magnitude and $\kappa := |\log \delta|$ describing its exponential growth as a function of m, n.

It follows from (12) and (17) that

$$a_{m,n}^{\text{meas}} = \epsilon \hat{h}_{m+n} + \sigma W_{m,n} + \epsilon^2 V_{m,n}^{\epsilon},$$

where $V_{m,n}^{\epsilon}$ denotes the approximation error. Therefore, introducing the estimator (for $p \geq 2$):

$$\hat{h}_p^{\text{est}} = \frac{1}{\epsilon} \sum_{n=1}^{p-1} \frac{1}{(p-n)n} a_{p-n,n}^{\text{meas}}$$

yields

$$\hat{h}_p^{\text{est}} = \hat{h}_p + \frac{\sigma}{\epsilon} \widetilde{W}_p + \epsilon \widetilde{V}_p^{\epsilon}, \tag{19}$$

with

$$\widetilde{W}_p = \frac{1}{(p-1)} \sum_{n=1}^{p-1} \frac{1}{(p-n)n} W_{p-n,n}, \tag{20}$$

$$\widetilde{V}_p^{\epsilon} = \frac{1}{(p-1)} \sum_{n=1}^{p-1} \frac{1}{(p-n)n} V_{p-n,n}^{\epsilon}. \tag{21}$$

Note that the independent standard complex circularly symmetric Gaussian random variables $\widetilde{W}_p$ are such that

$$\mathbb{E}[|\widetilde{W}_p|^2] = \frac{1}{(p-1)^2} \Big[\sum_{n=1}^{p-1} \frac{1}{n^4 (p-n)^4} \Big] \exp[2\kappa p] \overset{p \gg 1}{\simeq} \frac{\pi^4}{45 p^6} \exp[2\kappa p]. \tag{22}$$

We assume that $\epsilon^2 \ll \sigma$, which insures that the measurement errors in the contracted GPTs dominate the approximation error, and introduce the signal-to-noise ratio (SNR):

$$\text{SNR} = (\frac{\epsilon}{\sigma})^2.$$

We can see from (19) and (22) that in order to resolve the pth mode $\hat{h}_p$ of h, for $p \leq 2N$, we need the following resolving condition to be satisfied [1]:

$$N < \frac{1}{2\kappa} \ln \text{SNR}, \tag{23}$$

provided that $\hat{h}_p, p \leq 2N$ are of order one. This shows that a very high SNR is needed if one wishes to resolve the high order modes of the perturbation h. Furthermore, since κ is a decaying function of δ, we get the expected result that it is more difficult to estimate the high order modes of the perturbation h as the radius δ of the inclusion is smaller.

6 GPTs matching approach

6.1 Minimization algorithm

Let D be an unknown domain, which could be a cluster of separated inclusions as in Section 4. We let $M_{\alpha\beta}(\lambda, D)$ denote the GPTs associated with $D = \cup_{j=1}^{J} D_j$ and $\lambda = (\lambda_1, \dots, \lambda_J)$.

Suppose that $M_{\alpha\beta}(\lambda, D)$ are known for all $|\alpha|+|\beta| \leq N$ for some number N. We reconstruct the location and the shape of D by minimizing the discrepancy between the given and simulated GPTs. In [9], a recursive algorithm to approximate the shape of D is proposed. The recursive optimization procedure is to minimize over B for $l = 3, \ldots, N$,

$$\mathcal{J}^{(l)}[B] := \frac{1}{2} \sum_{|\alpha|+|\beta|\leq l} \left| \sum_{\alpha,\beta} a_\alpha b_\beta M_{\alpha\beta}(\lambda, B) - \sum_{\alpha,\beta} a_\alpha b_\beta M_{\alpha\beta}(\lambda, D) \right|^2 . \tag{24}$$

Here the coefficients (a_α) and (b_β) are such that $H(x) = \sum a_\alpha x^\alpha$ and $F(x) = \sum b_\beta x^\beta$ are homogeneous harmonic polynomials. At step l one uses as an initial guess the result of step $l-1$. At the first step ($l = 3$) one gets an equivalent ellipse as well as the location of the domain [9].

Note that using definition (7) of the contracted GPTs, one can see that minimizing $\mathcal{J}^{(l)}$ is equivalent to minimizing

$$\mathcal{J}_c^{(l)}[B] := \frac{1}{2} \sum_{n+m\leq l} \left| M_{nm}^c(\lambda, B) - M_{nm}^c(\lambda, D) \right|^2 . \tag{25}$$

To minimize $\mathcal{J}^{(l)}[B]$ we need to compute the shape derivative, $d_S\mathcal{J}^{(l)}$, of $\mathcal{J}^{(l)}$, which it can be obtained easily using (14). Suppose that B has J' components, *i.e.*, $B = \cup_{j=1}^{J'} B_j$, and the conductivity of B_j is k_j. Let $h = (h_1, \ldots, h_{J'})$ be the functions determining the deformation of ∂B_j, $j = 1, \ldots, J'$. Let

$$w_j^{HF}(x) = (k_j - 1) \left[\frac{\partial u}{\partial \nu}\Big|_- \frac{\partial v}{\partial \nu}\Big|_- + \frac{1}{k_j} \frac{\partial u}{\partial T}\Big|_- \frac{\partial v}{\partial T}\Big|_- \right](x), \quad x \in \partial B_j$$

where u and v satisfy (15) and (16) with D replaced by B, respectively. From (14) the shape derivative of $\mathcal{J}^{(l)}$ at B in the direction of h is given by

$$\langle d_S\mathcal{J}^{(l)}[B], h \rangle = \sum_{|\alpha|+|\beta|\leq l} \delta_{HF} \sum_{j=1}^{J'} \langle w_j^{HF}, h_j \rangle_{L^2(\partial B_j)}, \tag{26}$$

where

$$\delta_{HF} = \sum_{\alpha,\beta} a_\alpha b_\beta \big(M_{\alpha\beta}(\lambda, B) - M_{\alpha\beta}(\lambda, D) \big).$$

It is worth mentioning that the only information about h_j which is used in formula (26) is the projections onto the space spanned by w_j^{HF}.

If the target domain D is connected (and consequently all the domains B under consideration are connected), one can modify the earlier shape B to obtain B^{mod} for the next step by applying the gradient descent method:

$$\partial B^{\mathrm{mod}} = \partial B - \left(\frac{\mathcal{J}^{(l)}[B]}{\sum_{H,F} \left(\langle d_S\mathcal{J}^{(l)}[B], w^{HF} \rangle \right)^2} \sum_{H,F} \langle d_S\mathcal{J}^{(l)}[B], w^{HF} \rangle w^{HF} \right) \nu, \tag{27}$$

where ν is the outward unit normal to B. This procedure was implemented in [9] and computational results there clearly show that fine details of the shape can be reconstructed provided that the domain is connected.

In the same paper the procedure is applied to detect the domain with multiple components. The results show that the process can create shapes approaching the target shape, but not changing topology. In order to be able to change topology and reconstruct domains with multiple components, we develop a level-set version of the matching GPTs procedure described below.

6.2 Level-set framework

Adopting the level-set framework, one can change the topology in the shape reconstruction. See, for instance, [23, 14]. Hence, one can reconstruct the cluster of inclusions $D = \cup_j D_j$ without knowing the number J of separated components of D in advance.

Initial guess. Given $M_{\alpha\beta}$ for $|\alpha| = |\beta| = 1$ (called PT for polarization tensor), one can find an (equivalent) ellipse with the same PT but not its location since the PT is invariant under translation. One can locate this ellipse provided that its GPTs with $|\alpha| + |\beta| = 3$ are known, and it provides a good initial guess. The method is explained in detail in [4] and [9].

Recursive scheme. Within the level set framework, one represents ∂B as the zero level set of a continuous function ϕ so that $B = \{\phi < 0\}$.

As (27), one converts the minimization problem of (24) into a level set form by choosing the gradient ascent direction $V(x)$ on $x \in \partial D_j$ as

$$V(x) = \frac{\mathcal{J}^{(l)}[B]}{\sum_{H,F} \sum_{j=1}^{J'} \left(\langle d_S \mathcal{J}^{(l)}[B], w_j^{HF}[B]\chi_{\partial D_j} \rangle \right)^2} \sum_{H,F} \langle d_S \mathcal{J}^{(l)}[B], w_j^{HF}[B]\chi_{\partial D_j} \rangle w_j^{HF}[B](x), \tag{28}$$

for each $j = 1, \ldots, J'$. We can simply set

$$V(x) = \sum_{H,F} \alpha_j^{HF}[B] w_j^{HF}[B](x), \tag{29}$$

where α_j^{HF} is defined by (28). Then we evolve ϕ by solving the Hamilton-Jacobi equation

$$\frac{\partial \phi}{\partial t} + V|\nabla\phi| = 0, \tag{30}$$

for one time step.

It is worth emphasizing that in (29), V is only defined on the boundary ∂B, even though under the level set framework it has to be defined on the whole domain. Since $\nu = \nabla\phi/|\nabla\phi|$, we can modify w_j^{HF} as

$$w_j^{HF}[B]|_- = (k_j - \frac{1}{k_j}) \left(\nabla v[B]|_- \cdot \frac{\nabla\phi}{|\nabla\phi|} \right) \left(\nabla u[B]|_- \cdot \frac{\nabla\phi}{|\nabla\phi|} \right) + (1 - \frac{1}{k_j}) \nabla v[B]|_- \cdot \nabla u[B]|_-, \tag{31}$$

and

$$w_j^{HF}[B]|_+ = (-1 + \frac{2}{k_j} - \frac{1}{k_j^2}) \left(\nabla v[B]|_+ \cdot \frac{\nabla\phi}{|\nabla\phi|} \right) \left(\nabla u[B]|_+ \cdot \frac{\nabla\phi}{|\nabla\phi|} \right) + (1 - \frac{1}{k_j}) \nabla v[B]|_+ \cdot \nabla u[B]|_+, \tag{32}$$

where u and v satisfy (15) and (16), respectively (with D replaced with B).

7 Numerical experiments

In this section, we perform some numerical experiments of recovering the shape of a domain from its GPTs. In all of the numerical examples presented in this section, we apply the level set approach presented in the previous section. We emphasize that we do not make any a priori assumption on the number of connected components of the domain.

In order to acquire the GPTs, we solve the boundary integral equation (1) numerically; see [9] for more detailed explanation. All the λ_j are set to be 1 except in Example 6.

Example 1. Figure 1 shows that the equivalent ellipse is separated into 2 pieces and gradually modified toward the target domain. The first image is the equivalent ellipse and the others are the reconstructed images after $20, 30, 40, 70, 90$ iterations. Figure 2 is the graph of the relative area difference $\frac{|D \triangle B|}{|D|}$, where B is the reconstructed domain.

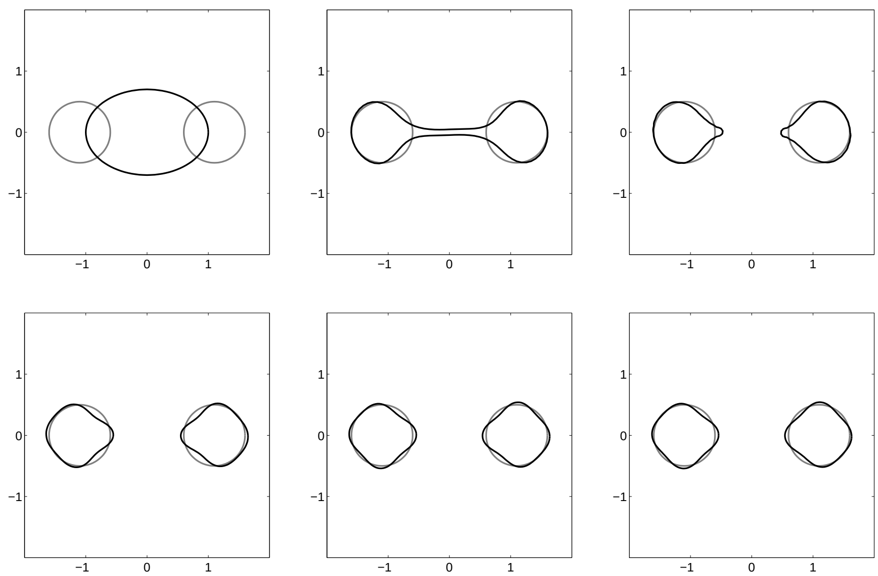

Figure 1: The GPTs of order $N = 4$, *i.e.*, $M_{\alpha\beta}$ with $2 \leq |\alpha| + |\beta| \leq 4$, separate the inclusion of 2 pieces. The first image is the equivalent ellipse and the others are the reconstructed images after $20, 30, 40, 70, 90$ iterations. The gray curve is the target domain and the black curve is the reconstructed one.

Example 2. The example in Figure 3 shows the reconstruction of the 3 inclusions D using $M(1, D) + \mathcal{E}$, instead of $M(1, D)$, with various relative noise $\mathcal{E}$ with

$$\frac{\left(\sum_{|\alpha|+|\beta|\leq 6}(\sum a_\alpha b_\beta \mathcal{E}_{\alpha\beta})^2\right)^{\frac{1}{2}}}{\left(\sum_{|\alpha|+|\beta|\leq 6}(\sum a_\alpha b_\beta M_{\alpha\beta})^2\right)^{\frac{1}{2}}} = 0,\ 0.1,\ 0.2.$$

Here we use GPTs up to order 6, *i.e.*, $N = 6$.

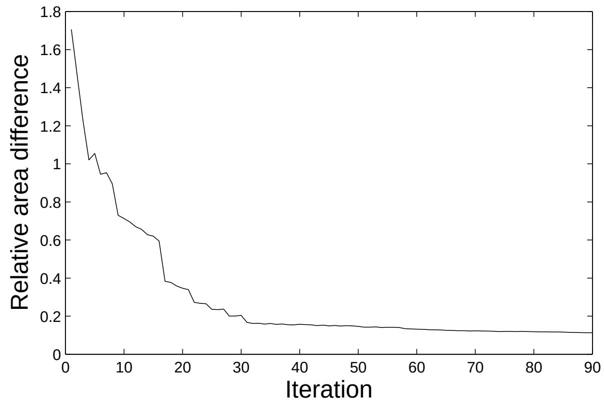

Figure 2: The relative area difference of the example in Figure 1.

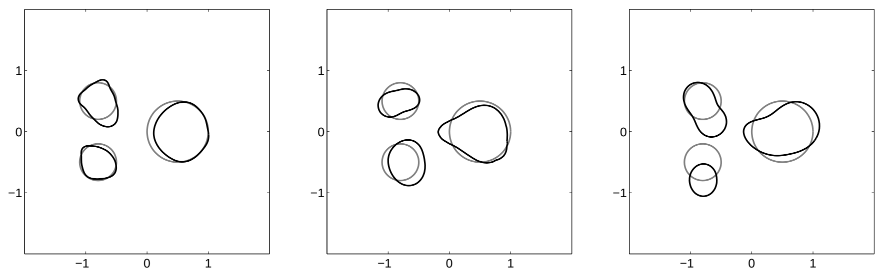

Figure 3: Reconstructed images after 150 iterations using GPTs of order up to $N = 6$. The first, second and third figure is from the data with 0%, 10%, 20% relative noise, respectively.

Example 3. This example is to demonstrate that the more components the target has, the higher GPTs are required to separate them. Figure 4 shows that one can not separate two components using $N = 3$, while $N = 4$ can. Similarly, one cannot separate 3 and 4 inclusions using the GPTs of order up to $N = 4$ and $N = 5$, respectively, see Figure 5 and Figure 6. Figure 7 shows that the GPTs needed to separate multiple inclusions depends on not only the number of inclusions but also their placement. In fact, using GPTs up to $N = 5$ may not be enough to separate 3 inclusions.

Example 4. Figure 8 shows that if two inclusions are located too close, one cannot separate them. It turned out from the numerical simulations that one cannot separate two disks of radius 0.5 using the GPTs of order up to $N = 6$ if the distances between them are smaller than 0.38.

Example 5. High-frequency information is undetectable, see Figure 9.

Example 6. Even when λ_j of the inclusions D_j are different, one can separate 4 inclusions using the GPTs of order up to $N = 6$ if they have the same signs. In Figure 10, the λ_j of left,

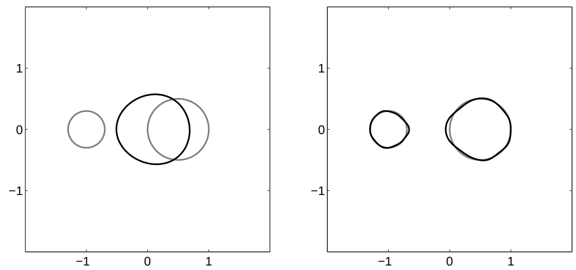

Figure 4: Reconstructed images after 70 iterations. The first figure is obtained using GPTs of order up to $N = 3$, and the second is of order up to $N = 4$. GPTs of order up to $N = 3$ cannot separate 2 inclusions.

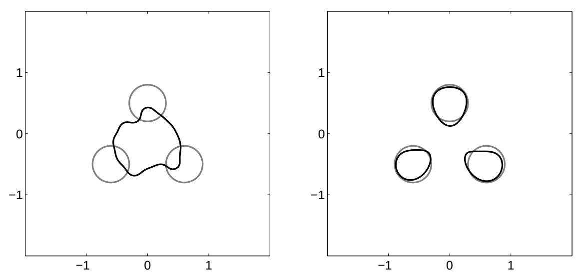

Figure 5: Reconstructed images after 100 iterations. The first figure is obtained using GPTs of order up to $N = 4$, and the second is of order up to $N = 5$. GPTs of order up to $N = 4$ cannot separate 3 inclusions.

bottom, right, and top inclusions are $1, 1, 11/18, 15/26$, respectively. For reconstruction we use $\lambda = 1$. If λ_j have different signs, some of them may not be detected. This phenomenon is closely related to our construction of GPTs vanishing structures in [8]. For example, when we reconstruct in Figure 11 inclusions assuming $\lambda = 1$, the ones with negative λ are undetectable.

8 Conclusion

In this paper we have presented a new approach for shape description and matching. Our approach is based on a novel global shape descriptor, the notion of GPTs. Compared to moments, which provide a region descriptor, the GPTs can be viewed as a boundary descriptor. We have performed numerical simulations to demonstrate that GPTs capture both high frequency shape oscillations and topology. Moreover, the notion of GPTs gives a natural hierarchical shape distance. The discrepancy between the contracted GPTs, M^c_{mn} for $m, n \leq N$, associated to two clutters of inclusions measure the similarity between them. Higher is N, better is the correspondence between the high-frequency details in the two clutters. This will be used in a forthcoming work for target recognition from wave imaging

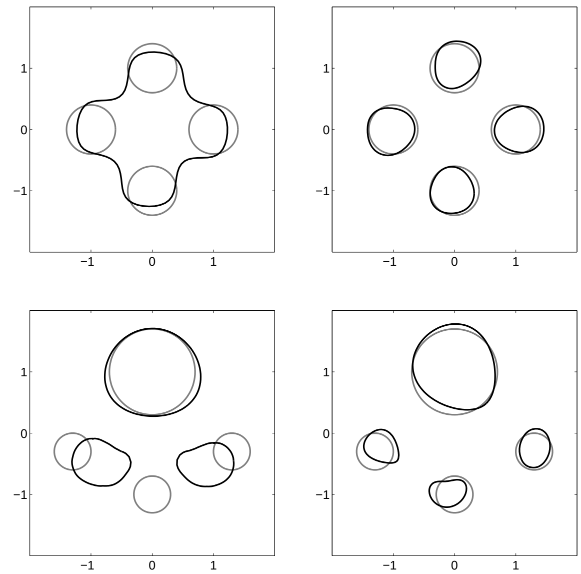

Figure 6: The first and second columns are reconstructed images after 400 iterations using GPTs of order up to $N = 5$ and $N = 6$, respectively. GPTs of order up to $N = 5$ cannot separate 4 inclusions.

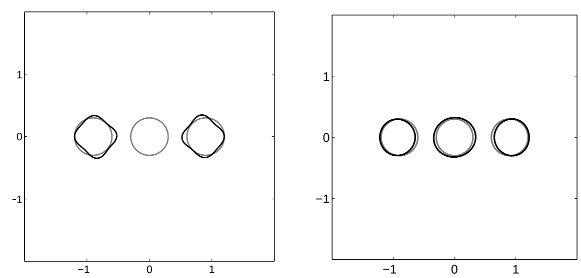

Figure 7: Reconstructed images after 100 iterations. The first figure is obtained using GPTs of order up to $N = 5$, and the second is of order up to $N = 6$. The number of GPTs needed to separate multiple inclusions depends on not only the number of inclusions but also their placement.

data. As shown in [10], GPTs can be accurately obtained from (multistatic) wave measurements by solving a linear system. Therefore, it would be very interesting in wave imaging to design a fast algorithm which identifies a target using a dictionary of precomputed GPTs data. Another challenging problem is to understand the relationship between the number of connected components of a target and the number of GPTs needed to separate them. It would be very interesting to find a formula for the number of GPTs needed to separate multiple disk-shaped inclusions as function of their number, radii, and the distances between

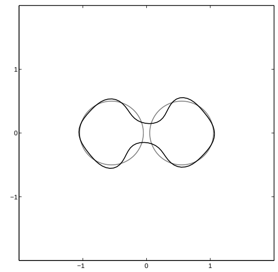

Figure 8: Reconstructed image after 100 iterations using GPTs of order up to $N = 6$. When two inclusions are located too close, one cannot separate them.

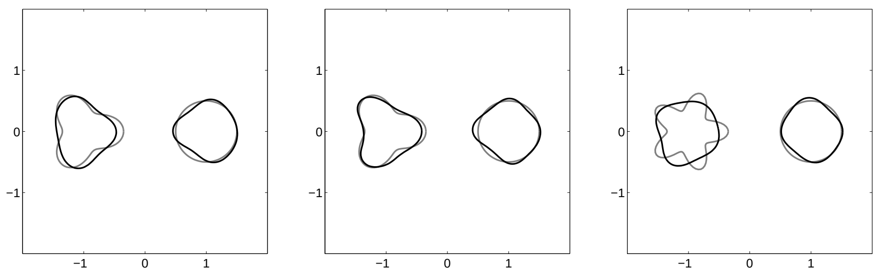

Figure 9: The first, second, and third figure is the reconstructed image using the GPTs of order up to 4, 5, and 7, respectively. High-frequency (compared to the GPTs order) perturbation is undetectable.

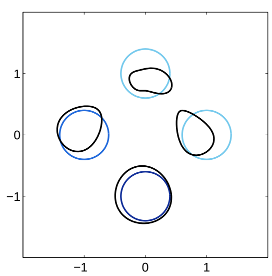

Figure 10: Reconstructed image after 400 iterations using the GPTs or order up to $N = 6$. The λ_j of left, bottom, right, and top inclusions are $1, 1, 11/18, 15/26$, respectively.

them.

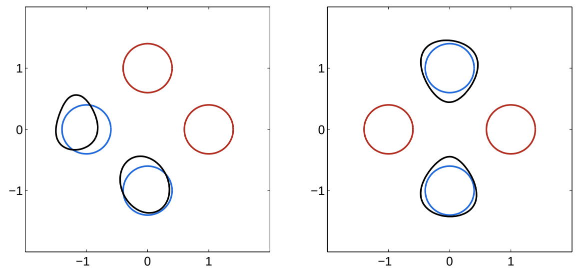

Figure 11: Reconstructed images after 400 iterations using the GPTs of order up to $N = 6$. The λ_j of red and blue colors are $-1.5, 11/14$, respectively. For reconstruction we use $\lambda = 1$. Inclusions of negative λ are undetectable.

References

[1] H. Ammari, J. Garnier, and K. Sølna, Resolution and stability analysis in linearized conductivity and wave imaging. Part I: Full aperture case, Proc. Amer. Math. Soc., submitted.

[2] H. Ammari and H. Kang, High-order terms in the asymptotic expansions of the steady-state voltage potentials in the presence of conductivity inhomogeneities of small diameter, SIAM J. Math. Anal., 34 (2003), 1152–1166.

[3] H. Ammari and H. Kang, Properties of generalized polarization tensors, SIAM Multiscale Model. Simul., 1 (2003), 335–348.

[4] H. Ammari and H. Kang, *Reconstruction of Small Inhomogeneities from Boundary Measurements*, Lecture Notes in Mathematics, Vol. 1846, Springer-Verlag, Berlin, 2004.

[5] H. Ammari and H. Kang, *Polarization and Moment Tensors with Applications to Inverse Problems and Effective Medium Theory*, Applied Mathematical Sciences, Vol. 162, Springer-Verlag, New York, 2007.

[6] H. Ammari, H. Kang, E. Kim, and M. Lim, Reconstruction of closely spaced small inclusions, SIAM J. Numer. Anal., 42 (2005), 2408–2428.

[7] H. Ammari, H. Kang, and M. Lim, Polarization tensors and their applications, *Proceedings of the second International Conference on Inverse Problems: recent developments and numerical approaches, Shanghai, 2004*, Journal of Physics: Conference Series, 12 (2005), 13–22.

[8] H. Ammari, H. Kang, M. Lim, and H. Lee, Enhancement of near-cloaking using generalized polarization tensors vanishing structures. Part I: The conductivity problem, Commun. Math. Phys., submitted.

[9] H. Ammari, H. Kang, M. Lim, and H. Zribi, The generalized polarization tensors for resolved imaging. Part I: Shape reconstruction of a conductivity inclusion, Math. Of Comp., 81 (2012), 367–386.

[10] H. Ammari, H. Kang, E. Kim, and J.-Y. Lee, The generalized polarization tensors for resolved imaging. Part II: Shape and electromagnetic parameters reconstruction of an electromagnetic inclusion from multistatic measurements, Math. Of Comp., to appear.

[11] H. Ammari, H. Kang, G. Nakamura, and K. Tanuma, Complete asymptotic expansions of solutions of the system of elastostatics in the presence of inhomogeneities of small diameter, J. Elasticity, 67 (2002), 97–129.

[12] H. Ammari, H. Kang, and K. Touibi, Boundary layer techniques for deriving the effective properties of composite materials, Asymp. Anal., 41 (2005), 119–140.

[13] M. Brühl, M. Hanke, and M.S. Vogelius, A direct impedance tomography algorithm for locating small inhomogeneities, Numer. Math., 93 (2003), 635–654.

[14] M. Burger and S.J. Osher, A survey on level set methods for inverse problems and optimal design, European J. Appl. Math., 16 (2005), 263–301.

[15] Y. Capdeboscq, A. B. Karrman, and J.-C. Nédélec, Numerical computation of approximate generalized polarization tensors, Appl. Anal., to appear.

[16] G.B. Folland, *Introduction to Partial Differential Equations*, Princeton University Press, Princeton, New Jersey, 1976.

[17] A. Friedman and M.S. Vogelius, Identification of small inhomogeneities of extreme conductivity by boundary measurements: a theorem on continuous dependence, Arch. Rat. Mech. Anal., 105 (1989), 299–326.

[18] A. Goldenshluger and V. Spokoiny, On the shape-from-moments problem and recovering edges from noisy Radon data, Prob. Theory Relat. Fields, 128 (2004), 123–140.

[19] A. Goldenshluger and A. Zeevi, Recovering convex boundaries from blurred and noisy measurements, Annals Statis., 34 (2006), 1375–1394.

[20] S. Loncaric, A survey of shape analysis techniques, Pattern Recognition, 31 (1998), 983–1001.

[21] G.W. Milton, *The Theory of Composites*, Cambridge Monographs on Applied and Computational Mathematics, Cambridge University Press, 2001.

[22] G. Pólya and G. Szegö, *Isoperimetric Inequalities in Mathematical Physics*, Annals of Mathematical Studies Number 27, Princeton University Press, Princeton, NJ, 1951.

[23] F. Santosa, A level-set approach for inverse problems involving obstacles, ESAIM: COCV, 1 (1996), 17–33.

[24] M. R. Teague, Image analysis via the general theory of moments, J. Optical Soc. Amer., 70 (1980), 920–930.